ENVIRONMENTAL RESEARCH
LETTERS

PURPOSE-LED PUBLISHING™ Part of the ENVIRONMENTAL RESEARCH SERIES

LETTER • **OPEN ACCESS**

Dust source activation frequency across East Asia

To cite this article: Lingle Chen *et al* 2025 *Environ. Res. Lett.* **20** 074056

IOP Publishing Environ. Res. Lett. 20 (2025) 074056 https://doi.org/10.1088/1748-9326/addee6

ENVIRONMENTAL RESEARCH
LETTERS

OPEN ACCESS

RECEIVED
28 January 2025

REVISED
25 May 2025

ACCEPTED FOR PUBLICATION
30 May 2025

PUBLISHED
18 June 2025

LETTER

Dust source activation frequency across East Asia

Lingle Chen[1,*], **Kerstin Schepanski**[2], **Anya J Crocker**[1], **Chuang Xuan**[1] and **Paul A Wilson**[1]

[1] School of Ocean and Earth Science, University of Southampton, Waterfront Campus, National Oceanography Centre, Southampton, United Kingdom
[2] Freie Universität Berlin, Department of Earth Sciences, Institute of Meteorology, Berlin, Germany
[*] Author to whom any correspondence should be addressed.

E-mail: lingle.chen@soton.ac.uk

Keywords: East Asia, dust source activation, Himawari-8/9 imagery, land surface, the Tibetan Plateau

Supplementary material for this article is available online

Abstract

Plumes of mineral dust in East Asia deleteriously impact the health and livelihoods of hundreds of millions of people in Mongolia, China, Korea, and Japan and perturb Earth's energy balance and climate. However, the sources of this dust are not well-documented, limiting understanding of dust emissions. Here, we systematically quantify dust source activation frequency (DSAF) across East Asia (80–130° E; 27–52° N) between January 2016 and December 2023. Our data reveal a vast dust-active area extending from the Tibetan Plateau (TP) in the southwest to the Huin Bair Sandy Land in the northeast, but two regions dominate: southern sources centered on the margins of the Taklimakan Desert and northern ones centered on the valleys of the Gobi Desert. East Asia is most dust-active in boreal spring (46% of all recorded events). This seasonal peak is pronounced in northern sources where snow cover, vegetation and orographic/topographic influence on winds are clear controls on DSAF. The main southern sources are active year-round with DSAF hotspots attributable to desiccated lakes and riverbeds. The TP, commonly considered a sink for in-bound windblown dust, is also a dust source, particularly in winter, with emissions controlled by precipitation patterns, snow cover and wind funneling through deep river gorges. Contrary to suggestions, our data show that the Loess Plateau is not a major dust source. We document a marked increase in dust source activation during the 2020 extreme heat wave on the overgrazed Mongolian Plateau grasslands. Our data provide a framework to study past variability in the two-way climate interactions that control dust emissions on historical and geological timescales and a baseline from which to measure future change.

1. Introduction

The deserts of East Asia (figure 1) are a major supplier of mineral dust to the atmosphere (Ginoux *et al* 2004), emitting between 400 and 1000 teragrams (Tg) of dust annually (Kok *et al* 2021), with serious impacts on the health and livelihoods of hundreds of millions of people in Mongolia, northern China, Korea, and Japan (Shao and Dong 2006). Dust from East Asia is also transported vast distances to the North Pacific Ocean (Pye and Zhou 1989), North America (Zdanowicz *et al* 2006), and Greenland (Huang *et al* 2015), influencing cloud physics, regional radiation budgets and climates (Huang *et al* 2014). Yet the sources of this dust and the frequency of their activation have received less attention than atmospheric dust plumes and their transportation. Early studies of dust storm activity in East Asia used data from meteorological stations (Sun *et al* 2001, Qian *et al* 2002, Kurosaki and Mikami 2003, Wang *et al* 2005), the Total ozone mapping spectrometer absorbing aerosol index (Prospero *et al* 2002) and dust emission modeling (Xuan and Sokolik 2002, An *et al* 2018). Moderate resolution imaging spectroradiometer (MODIS) data, with twice-daily observations, have been employed to study dust activity in the Taklimakan and Gobi deserts (Zhang *et al* 2008, 2015a, Nobakht *et al* 2021) and stereo imaging

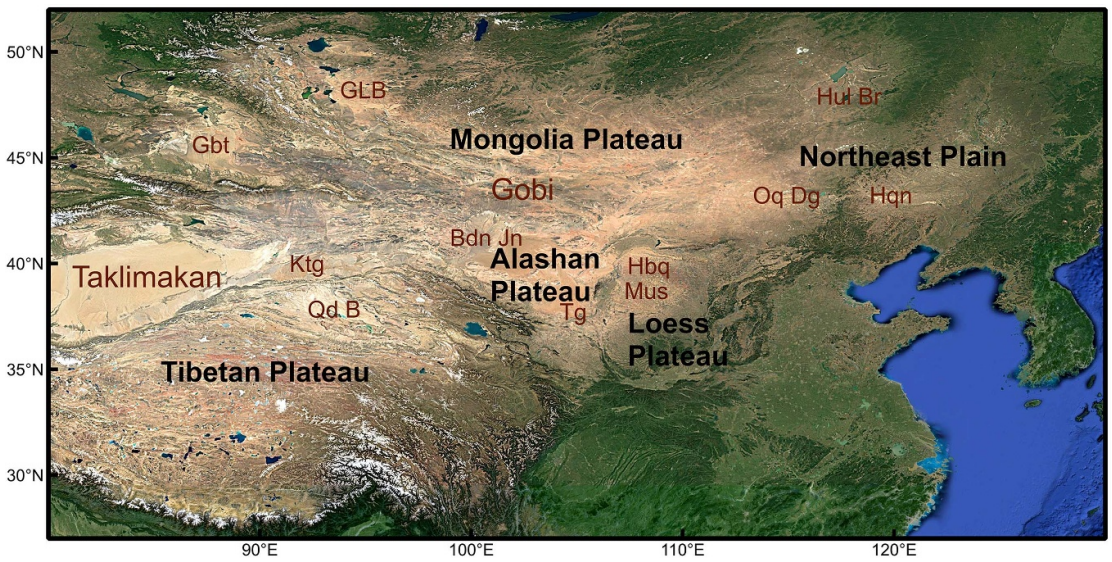

Figure 1. Study region with place names and geographic features mentioned in the text. Dust source active regions are labeled in brown, and highland/lowland regions are highlighted in bold black. Key locations include the Mongolian Plateau, the Alashan Plateau, the Loess Plateau, the Tibetan Plateau, and the Northeast Plain. The two primary dust source activation centers, the Taklimakan and the Gobi Deserts, are highlighted in brown. Secondary dust source regions include the Great Lake Basin (GLB), the Gurbantunggut Desert (Gbt), the Hulun Buir Sandy Land (Hul Br), the Onqin Daga Sandy Land (Oq Dg), the Horqin Sandy Land (Hqn), the Kumtag Desert (Ktg), the Baidan Jaran Desert (Bdn Jn), the Tengger Desert (Tg), the Qaidam Basin (Qd B), the Hobq Desert (Hbq), and the Mu Us Sandy Land (Mus). The base map is sourced from Google Earth ©.

from the Multi-angle Imaging Spectro Radiometer has been used to trace East Asian dust plume motion every 6–7 d (Yu *et al* 2019). However, in data sets of such limited temporal resolution, dust transport in the atmosphere obscures the sources of these emissions and their activation frequency, thereby hindering assessment of mechanistic forcing.

A key advance in pinpointing dust sources was provided by the thermal infrared radiance data from the Metaset second generation Spinning enhanced visible and infrared imager, which offers 15 min temporal resolution and has been used to track dust emissions to their sources across North Africa (Schepanski *et al* 2007), the Arabian Peninsula (Hennen *et al* 2019), and the Horn of Africa (Kunkelova *et al* 2024). For East Asia, the new-generation geostationary meteorological satellites Himawari-8/9 provide similar capabilities. The potential of this approach is demonstrated by studies of individual dust events originating from the Gobi Desert and northeastern China (Altausen *et al* 2019, Kai *et al* 2021) and the Taklimakan Desert (TK) (Yumimoto *et al* 2019). However, a comprehensive assessment of dust source activity across East Asian is lacking.

Here, we utilize high-spatiotemporal-resolution dust RGB imagery from the Himawari-8/9 satellites to (i) present the first detailed high-resolution DSAF record of East Asia (80–130° E, 27–52° N); (ii) examine the seasonality of East Asian dust source activations; and (iii) evaluate the land surface conditions that promote dust source activation.

2. Methodology

High-resolution spatiotemporal remote sensing satellite data from Himawari-8/9 were used to identify dust source activation from January 2016 through December 2023 (8 years). Himawari-8/9 is a new-generation geostationary meteorological satellite launched by the Japan Meteorological Agency (Bessho *et al* 2016). Himawari-9 began its backup operations for Himawari-8 in March 2017 and officially took on the primary operational role in December 2022. The Advanced Himawari Imager sensor aboard these platforms features 16 wavelength bands (channels): channel 1–3 images in the visible part of the spectrum, channel 4–6 the near-infrared, and channel 7–16 the far-infrared wavelength bands. The geospatial monitoring range of Himawari-8/9 is from 85° E to 160° W and from 60° N to 60° S. The spatial resolution is 2 km × 2 km (up to 0.5 km per pixel in the visible spectrum), and the temporal resolution is 10 min over East Asia.

We applied the Dust RGB method to convert Himawari-8/9 far-infrared channels to dust composite images (Akihiro 2020). This method takes advantage of the difference in reflection and transmission characteristics between atmospheric dust and other substances (e.g. low/mid/high-level cloud, and cold/warm deserts). Three infrared channels, i.e. 11, 13, and 15 are processed as follows: red (BT15–BT13), green (BT13–BT11), and blue (BT13). Areas with bright magenta or pinkish shading are recorded as

dust, tan–brown colors as clouds, and light cyan or light green as warm or cold deserts (supplementary figure 1). Smoke is not detected by dust RGBs because they use only IR bands. While dust and volcanic ash may appear similar in RGB, our study region is not an active volcanic zone or under the influence of advected volcanic ash plumes. Areas that emit dust were identified visually and marked as dust source activation events on a 1° × 1° gridded record covering East Asian deserts, spanning 80–130° E, 27–52° N. We generated 420 768 dust composite images covering an 8 year period (January 2016 to December 2023) and grouped them into 2,922 daily animations to enable rapid manual identification of dust plumes. We tracked 21 829 individual dust plumes (pinkish shading in the animation) back to their points of origin. Manual identification and calculations of DSAF follow the method of Schepanski *et al* (2007):

$$\text{DSAF}\ (\%) = \left({}^{N_s}/_{N_D}\right) \times 100.$$

N_s = total number of days with at least one dust event in 1° × 1° grid cell within a given interval,

N_D = number of days of available satellite observations within the same interval.

Note that DSAF indicates the timing and frequency but not the mass flux of dust emissions. Dust source identification is not possible under optically thick clouds or atmospheric dust layers. The pink shading of dust varies with surface emissivity, atmospheric moisture, atmospheric dust concentration and dust layer altitude (Banks *et al* 2019). Manual dust source identification necessarily introduces the potential for human error, but while we anticipate future improvements in automated algorithms, for now, skilled humans introduce fewer inconsistencies in their analyses of DSAF (AlNasser and Entekhabi 2024). To minimize subjective bias, we followed the protocol of Schepanski *et al* (2012) wherein all dust plumes were recorded but the modest subset (∼3% of total events) with an obscured source (e.g. because of cloud cover), were classified as uncategorized and excluded from our analysis to ensure a conservative and reliable estimate of dust activations.

3. Results and discussion

3.1. Spatial and seasonal characteristics of East Asian dust source activation

Our data reveal a vast area that is dust-active, extending from the Tibetan Plateau (TP) in the southwest to the Hulun Buir Desert in the northeast, and we identify two primary regions: a northern one, centered on the Gobi Desert and a southern one, centered on the TK (figures 1 and 2(a)). This result supports some interpretations from smaller data sets and model simulations (Prospero *et al* 2002, Xuan *et al* 2004, Zhang *et al* 2008, Ginoux *et al* 2012, Kim and Lee 2013), but the spatial and temporal granularity in our data permits precise identification of sources and mechanistic insight into dust generation. East Asia is most dust active in spring (46% of all events recorded) and least active in summer (14%) (figures 3(a) and (b)). We divide these two main source regions along 43° N, roughly corresponding to the southern limit of the Mongolian Plateau (figure 3). The northern region is most-active in spring (figure 3(d)) while the southern one, sandwiched between the TP and Mongolian Plateau, 36° N–43° N (figure 3(e)), is dust-active year-round (figure 3(f)). We also identify the TP (figure 3(g)) as a dust source, mostly active in winter and early spring (figure 3(h)). However, contrary to many suggestions (Xuan and Sokolik 2002, Xuan *et al* 2004) and in support of the opposing view (Kurosaki and Mikami 2003, Lim and Chun 2006), we show that the Loess Plateau (LP) is not an active present day dust source (figures 4 and 5).

A seasonal and latitudinal shift in atmospheric dust in East Asia has been inferred based on data from sparsely distributed meteorological stations (Han *et al* 2008). Our data show that, for half of the year (summer and autumn), the East Asia dust activation belt is centered on ∼40° N, in the southern source region (figure 4). In spring, high DSAF values extend to higher latitudes incorporating northern sources (figure 4(b)) where regional wind speeds also peak in spring (Shao and Dong 2006). In winter, the highest DSAF values are found at lower latitudes including the TP (figure 4(h)), implying the influence of the prevailing westerly jet over the TP (Schär *et al* 2009).

In spring, in addition to the Taklimakan and Gobi deserts, other northern sources, such as the Great Lake Basin (GLB), the northern Mongolian grasslands, and the Northeast Plain (NP), also contribute to dust emissions (figure 4(a)). The GLB on the northwestern Mongolian Plateau, home to one of the largest dune fields on the Mongolian Plateau, interconnected lakes, wetlands, and semi-arid landscapes (Lehmkuhl *et al* 2024), produces dust on ∼3% of spring days (figure 4(a)), a contribution that has not been clearly quantified before. Eastern Kazakhstan and the Gurbantunggut Desert (Gbt) also peak in dust source activation during spring, serving as minor contributors (figure 4(a)). This finding is consistent with the analysis of Nobakht *et al* (2021) who used twice-daily MODIS imagery, but we document more dust events in East Kazakhstan and the Gbt during non-spring months. In summer, the highest DSAFs are observed around the margins of the TK (figure 4(b)), and the Alashan Plateau (AP) is a secondary source (figure 4(c)). During autumn, the TK and the AP remain the dominant dust sources, but activation frequencies are lower (figure 4(e)). In

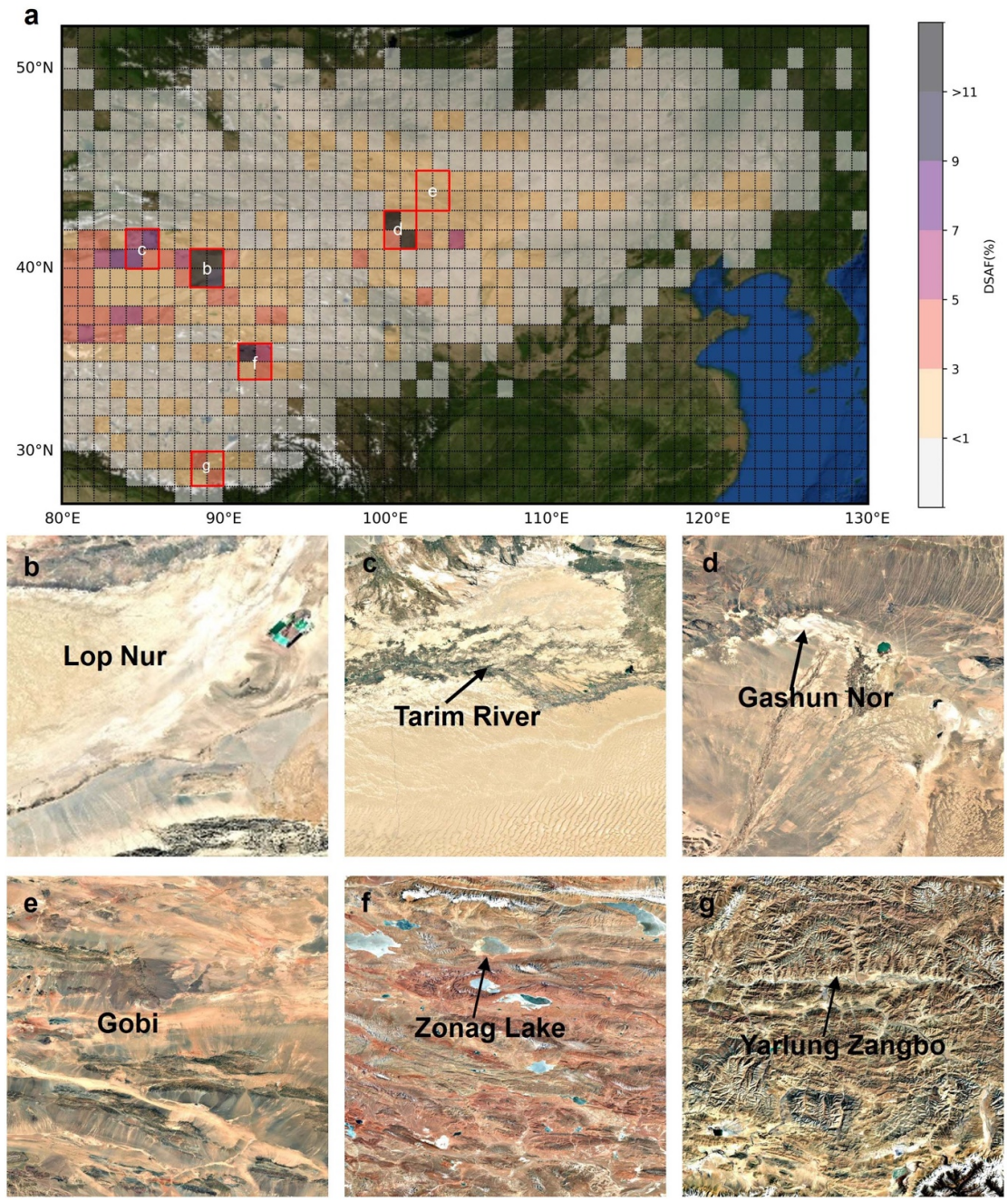

Figure 2. (a) Average annual dust source activation frequency (DSAF) from 2016 through 2023. The intensity of the color represents the DSAF percentage (darker shades = higher DSAF values). The small red (solid-line) boxes around areas of high DSAF indicate the full extent of the land surface images sourced from Google Earth © shown in panels b–g.

winter, dust source activation events are primarily concentrated on the TP, followed by the TK, the AP, the Qaidam Basin (Qd B) and the Ordos Plateau, which includes the Hobq Desert (Hbq) and the Mu Us Sandy Land (Mus) (figure 4(g)).

3.2. Land surface drivers of dust source activation

3.2.1. Dust hotspots in the taklimakan and gobi deserts

The highest DSAFs in East Asia occur in the southern source region, in the northeastern TK (figure 1), especially around Lake Lop Nur (figure 2(b), 89° E, 40° N), where dust activation occurs on ∼19% of days (figure 2(a)). This result is consistent with findings derived from the twice-daily MODIS imagery Nobakht *et al* (2021). While the date and cause of Lop Nur's desiccation are debated (Dong *et al* 2012), our data show that it is a hotspot of dust activity (figure 2(b)). The Tarim River and associated floodplains, located on the northern rim of the TK (figure 2(c), 80–90° E, 40–41° N) is also a significant dust source with activation on ∼7% of days (figure 2(a)). Glacial- and snow-melt from the Tianshan Mountains (Mts) are responsible for nearly 50% of annual river flow in the region (Chen *et al* 2006). The sediment transported during peak flow (summer ablation season) accumulates in loose, dry

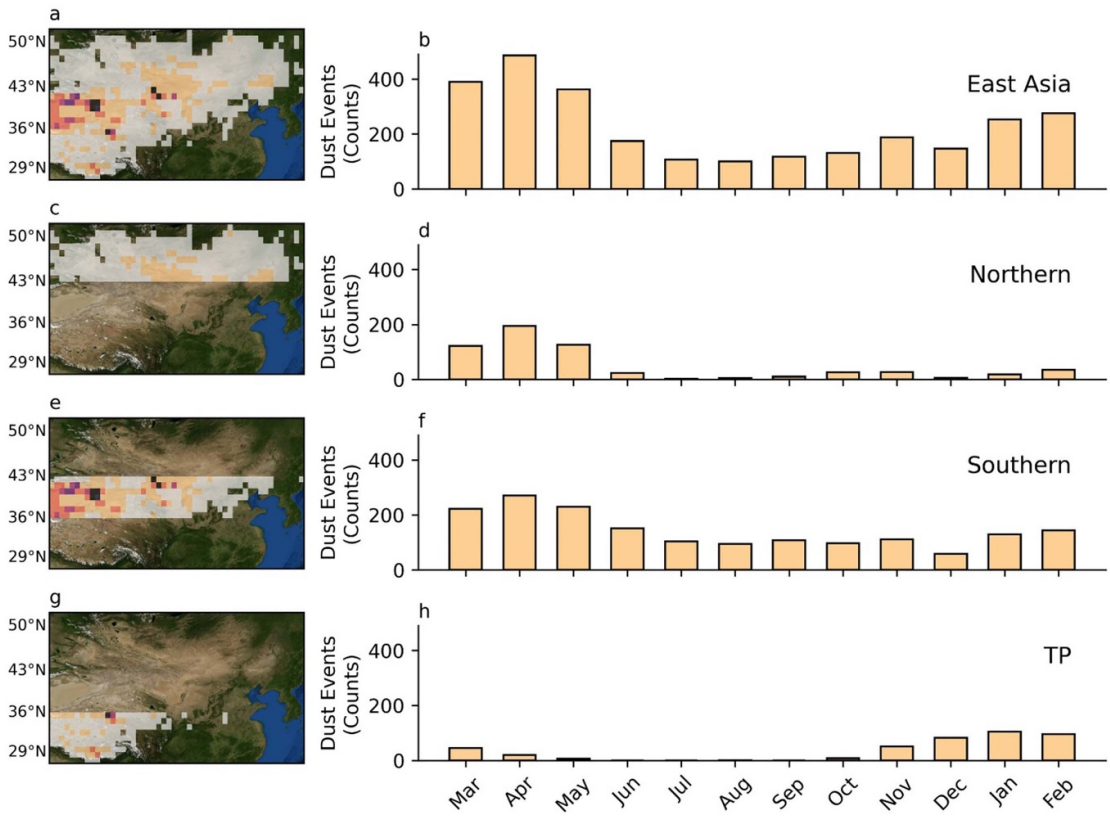

Figure 3. Monthly distribution of dust source activation (counts) for (a) East Asia (80–130° E; 27–52° N), (b) the northern source region (north of 43° N), (c) the southern source region (36° N–43° N), and (d) the Tibetan Plateau (TP, 27° N–36° N).

soils along the riverbanks making them highly susceptible to wind erosion when river levels fall prior to the next summer ablation season (Rittner *et al* 2016). Our data also show notable dust source activation along the southern rim of the Tarim Basin (80–85° E, 36–37° N, ∼6% of days), including the Hetian River (80–82° E, 36–41° N, ∼4% of days), which has not been clearly identified as an active dust source before (figure 2(a)). These rivers, fed by glacial- and snowmelt from Kunlun Mts, deposit sediment in alluvial fans, terminating in the central basin, where they desiccate during the dry season (Rittner *et al* 2016).

The most active area in the northern dust source region of East Asia is the southwestern Mongolian Plateau in the Gobi Desert (figures 1, 98–105° E, 42–45° N) where dust activation averages about 3% of days annually (figure 2(a)). The valleys of the Gobi-Altai Mountain ranges (figure 2(e), 100–103° E, 43–45° N) exhibit the highest DSAF, reaching ∼6% of spring days (figure 4(a)) across a landscape rich in lakes and paleolake remnants (Lehmkuhl *et al* 2018), which serve as abundant sources of fine-grained particles, readily mobilized by strong winds. This region is also characterized by orographic convergence and topographic funneling of synoptic winds, triggering dust events associated with the passage of Mongolian cyclones (Kai *et al* 2021).

3.2.2. The AP: A Year-Round Dust-Active Source

The AP (98–106° E, 38–42° N) and its adjacent regions, in western Inner Mongolia (northern China) (figure 1), is reportedly a source of dust storms (Sun *et al* 2001, Xuan and Sokolik 2002, Wang *et al* 2011) but, until now, its complex landscape with altitudes ranging from 820 m to around 1,500 m, deserts including the Badain Juran Desert, the Tengger Desert (Tg) and the Ulan Buh Desert, degraded oases and dried riverbeds (figure 5) made it challenging to discriminate dust sources (Wang *et al* 2019). Our data show that the AP is dust-active throughout the year (figure 5). Dust activation occurs on ∼3% of days (figure 5), peaking in spring (∼9% of spring days) (figures 3(c) and (d)) and desiccated water bodies are a key control. The southern side of the Altai Mts, particularly dry riverbeds in the Heihe Alluvial Plain (figures 5, 100–102° E, 41–42° N) and desiccated lakes such as Gashun Nor (dried in 1961) and Sugu Nor (dried in 1992) are suggested to be dust-active (Kurosaki and Mikami 2003, Natsagdorj *et al* 2003, Zhang *et al* 2008, Wu *et al* 2016). Our data reveal that Gashun Nor (figure 2(d), 100° E, 42° N) is the most dust-active source anywhere on the AP and the second most active source in all of East Asia, with ∼14% of days being dust-producing (figure 5) including ∼23% of spring days (figure 4(a)). The

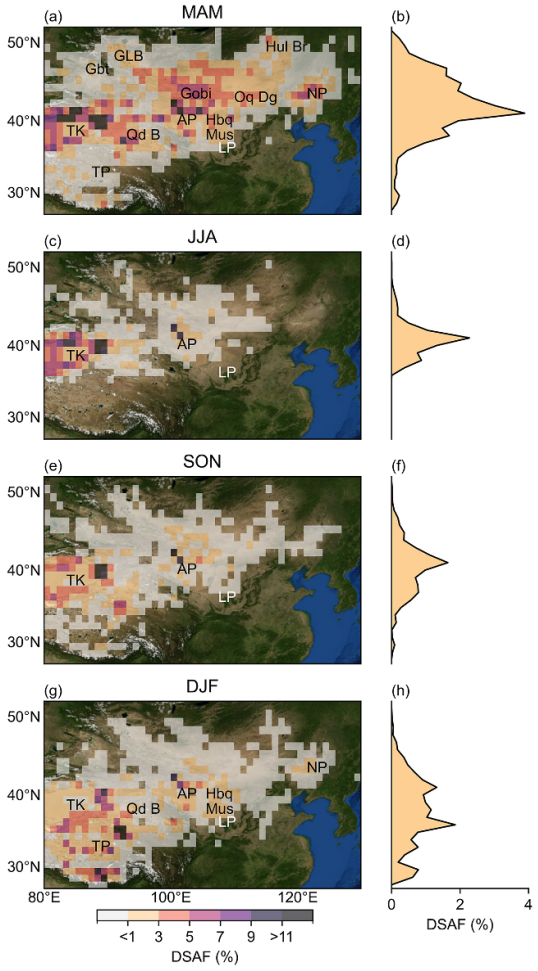

Figure 4. Seasonal latitudinal distribution of dust source activation frequency: (a)–(b) Spring (MAM, March, April, May), (c)–(d) Summer (JJA, June, July, August), (e)–(f) Autumn (SON, September, October, November), and (g)–(h) Winter (DJF, December, January, February). These frequencies are calculated from the recorded years between 2016 and 2023. Dust source regions labeled in black including: the Taklimakan Desert (TK), the Gobi Desert, the Great Lake Basin (GLB), the Gurbantunggut Desert (Gbt), the Hulun Buir Sandy Land (Hul Br), the Onqin Daga Sandy Land (Oq Dg), the Qaidam Basin (Qd B), the Hobq Desert (Hbq), the Mu Us Sandy Land (Mus), the Alashan Plateau (AP), the Tibetan Plateau (TP) and Northeast Plain (NP). The Loess Plateau (LP) is also indicated (in white because our data show that it is largely inactive, also see figure 5).

oasis areas along the Hexi Corridor (97–102° E, 38–41° N) are also important contributors with dust activation on ∼4% of days (figure 5) and ∼8% of spring days (figure 4(a)). Detrital materials from the Qilian Mts are transported by fluvial systems to the Hexi Corridor, supplying sediments that are well-suited for dust activation (Zhang *et al* 2022). Spring ploughing of croplands in these oasis regions leads to bare land with loosened surface sediments, reducing the threshold frictional velocity needed to trigger dust emission (Shen *et al* 2005).

The sandy deserts on the AP (e.g. the Badain Jaran Desert and the Tg) and the Ordos Plateau (e.g. the Hbq and the Mus) are much less dust-active (<1% of days) (figure 5). This result (i) suggests that interpretations from detailed case studies (Luo *et al* 2020, Wang *et al* 2021) are regionally applicable and (ii) is consistent with findings from North Africa (Schepanski *et al* 2007) and Arabia (Hennen *et al* 2019, Kunkelova *et al* 2022). We attribute it to a paucity of fine-grained sediments in these landscapes. Famously, the Chinese LP is a sink for wind-blown dust transported from elsewhere, but its role as a dust source is debated (Kurosaki and Mikami 2003, Xuan *et al* 2004). Our data show it to be a negligible modern day dust source (figure 5), a result we attribute to dense vegetation coverage and soils with high clay contents that promote aggregation and clodding (Xuan and Sokolik 2002).

3.2.3. The Mongolian Plateau and NP

3.2.3.1. Spring snow cover and vegetation

The Mongolian Plateau and adjacent regions (90–125° E, 43–52° N) exhibit pronounced seasonal variation in dust storms, vegetation and snow cover (Lee and Kim 2012). Vegetation increases surface roughness, reducing wind speeds and roots that bind soil particles, making them less likely to be entrained (Zender *et al* 2003). Snow inhibits dust emissions by blanketing potential dust source areas, by increasing the threshold wind velocity required for dust emission and by enhancing soil moisture after snowmelt (Kurosaki and Mikami 2004, Tanaka *et al* 2011). Our direct identification of dust sources enables a more precise evaluation of the role of snow cover and vegetation in modulating the spatiotemporal evolution of dust activation.

The Mongolian Plateau experiences a pronounced dust storm season that begins in February, intensifies during March and April and diminishes by May (Hao *et al* 2024). Our data show that DSAF is minimal in February (<3% the month's days) across the Mongolian Plateau, especially on its northern margin where extensive snow cover persists (figures 6(a) and (b)). Vegetation is limited in spring, but as snow gradually melts and retreats northward from February to April, DSAF increases significantly, peaking at 5%–7% of days in the month (figures 6(c)–(i)). In May, despite the absence of snow cover, the resurgence of vegetation in the northern and northeastern parts of the Mongolian Plateau leads to a significant decline in DSAF down to 1%–3% of the month's days (figures 6(j)–(l)). From 2016 to 2023 (February–May), dust source activation events (>1%) occurred when LAI ranged from 0.5 to 1.0, with snow cover below 20% (supplementary figure 2).

3.2.3.2. Human land use change

Global dust mass loading is suggested to have increased by ∼55% since pre-industrial times, with Asian dust contributing significantly to this change

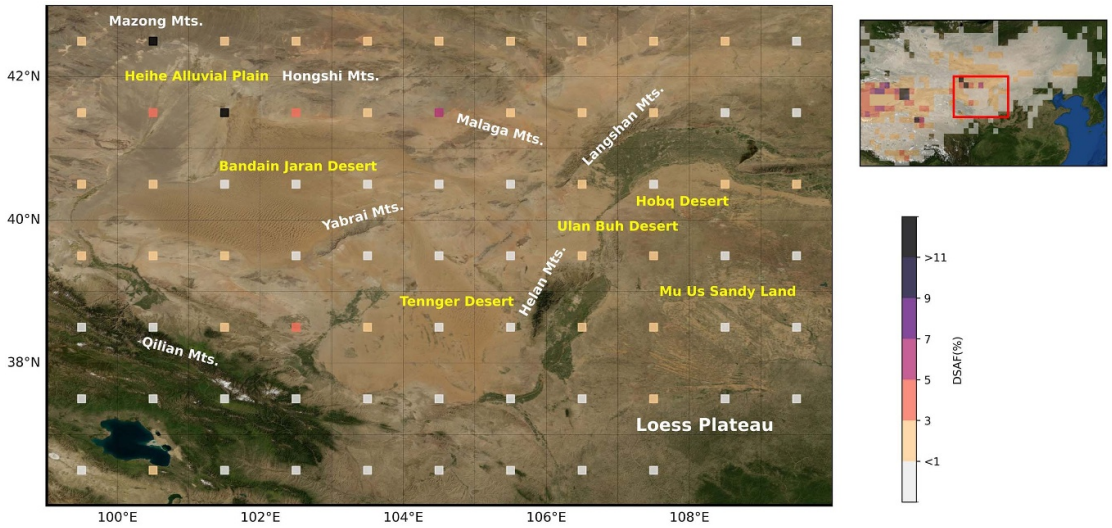

Figure 5. Annual dust source activation frequency (DSAF) on the Alashan Plateau and adjacent regions (see inset for location). DSAF for individual grid squares is shown as colored mini pixels. Dust active regions (i.e. deserts, sandy land, dry lake beds) are labeled in yellow. Mountains (Mts.) and plateaus are labeled in white. The underlying image is from NASA's Blue Marble: Shaded Relief.

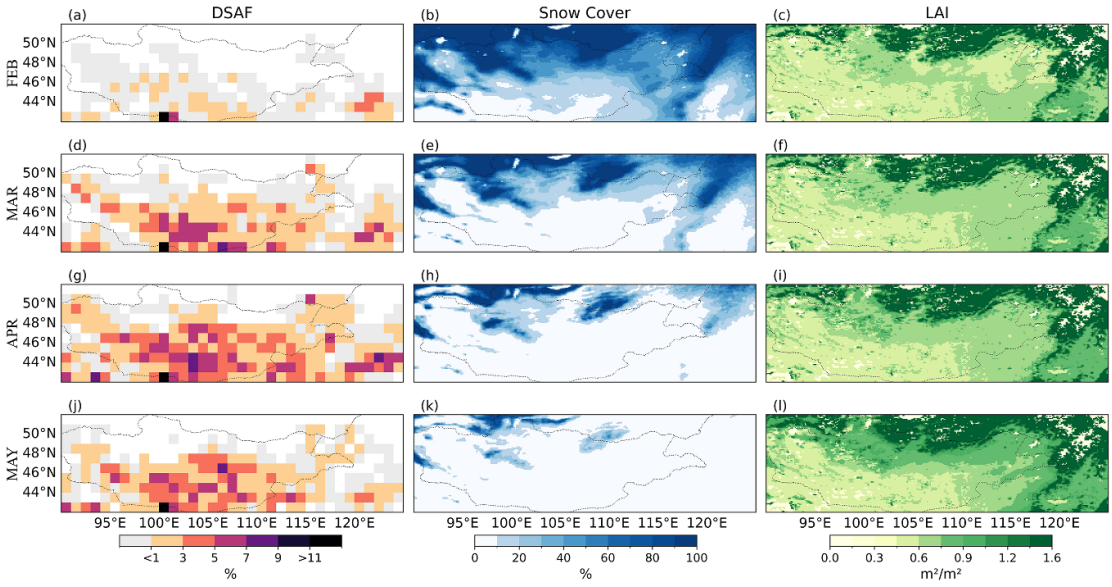

Figure 6. Dust source activation frequency (DSAF, left), snow cover (middle), and leaf area index (LAI, right) for the transition from winter to spring: February (FEB, a–c), March (MAR, d–f), April (APR, g–i), and May (MAY, j–l). Snow Cover and LAI index are reconstructed from European Centre for Medium-Range Weather Forecasts Reanalysis 5 (ERA5) data (average for 2016–2023).

(Kok *et al* 2023). However, current climate models fail to reproduce this increase, at least in part because they underestimate the influence on dust emissions of human-induced land use change which has been extensive in East Asia, especially on the Mongolian Plateau and the NP (Ginoux *et al* 2012). Today, the Mongolian Plateau and adjacent regions are characterized by three main land cover types: bare lands in the southwest, grasslands in the northeast and croplands in the east (figure 7). Our data show that the highest DSAFs are observed on bare lands on the southern Mongolian Plateau (activation on 3% $\sim$ 5% of days during the first half year) (figure 7(a)). The grasslands that lie immediately to the north, in central-eastern Mongolia, are also recognized as both a natural dust source area (Shinoda *et al* 2010) and, increasingly, as an area experiencing frequent droughts, leading to a reduction in vegetation cover and soil moisture (Nandintsetseg *et al* 2021) and grassland degradation driven by overgrazing by growing livestock populations (Nandintsetseg and Shinoda 2015). Our data show a spike in DSAF in this region during the first half of 2020 (figures 7(b) and (c)), the time of the record-breaking Siberian heatwave when the Verkhoyansk weather station recorded a daytime maximum of 38 °C on 20th June , the

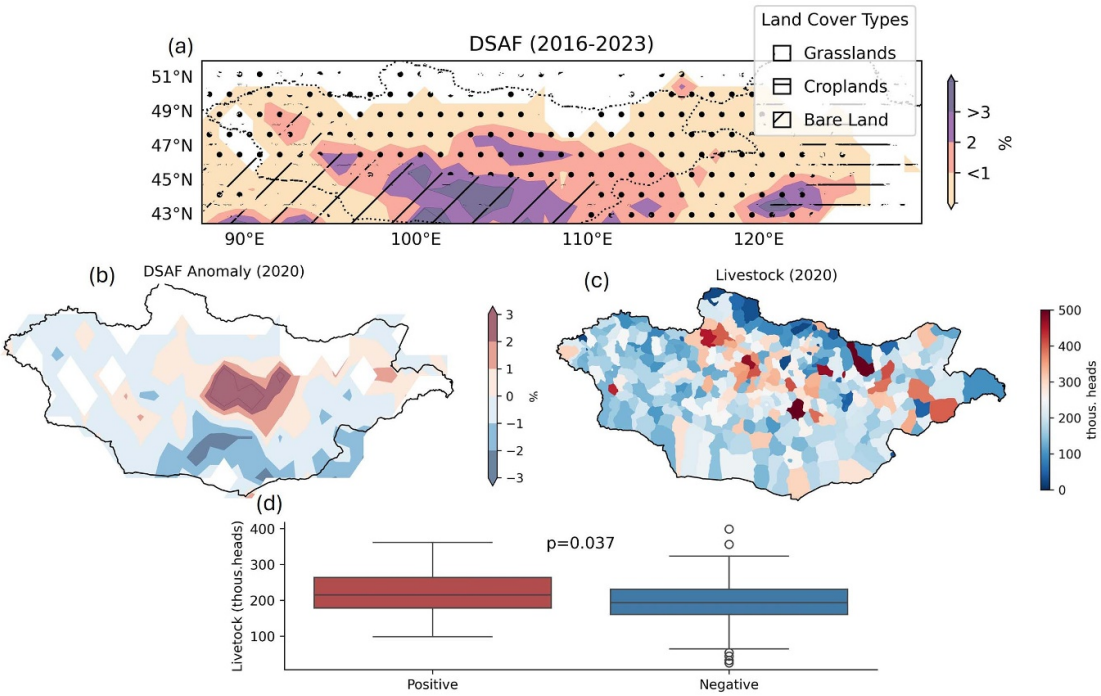

Figure 7. Response of Dust Source Activation Frequency (DSAF) to the extreme Siberian heatwave from January to June 2020. DSAF is shown in color (our data) and overlain with the average land cover (symbols) derived from MODIS MCD12C1 Version 6.1 data. Panel (a) displays DSAF from 2016–2023, panel (b) shows the 2020 anomaly (2020 minus the mean for 2016 through 2023), panel (c) shows livestock numbers in Mongolia for 2020 (the National Statistical Office of Mongolia, www.1212.mn/), panel (d) compares livestock numbers to the 2020 DSAF anomaly, with the *t*-test *p*-value shown in black. All panels use DSAF data for the January–June period, the time frame during which the 2020 heatwave was most strongly developed.

highest temperature ever recorded north of the Arctic Circle with abnormally warm temperatures extending onto the Mongolian Plateau (Ciavarella *et al* 2021). Furthermore, areas exhibiting a 2020-heatwave positive DSAF anomaly show higher livestock numbers compared to those with a negative 2020-heatwave DSAF anomaly (p-value = 0.037, figure 7(d)). These observations strongly suggest a human-induced land-surface control of the DSAF anomaly during the first half year of 2020 involving grazing-induced grassland degradation during extreme heatwave conditions.

Land use in NP is a mix of sandy lands (e.g. the Horqin Sandy Land, the Onqin Daga Sandy Land and Hulun Buir Sandy Land, figure 1), grasslands and croplands (figure 7(a)). Cropland extent has grown rapidly in northeast China in recent decades (Li *et al* 2004) and field studies suggest that these black soil croplands are a source of dust storms (Zhang *et al* 2015b). Our data support this suggestion, showing dust activation on ∼7% of spring days (figure 4(a)), presumably driven by strong winds during the ploughing season.

3.2.4. The TP: a winter-early spring dust active source

The TP is commonly regarded as a sediment sink for dust transported from elsewhere, but it is also suggested that it acts as a dust source (Zhang *et al* 2023), such as the Yarlung Zangbo River Valley (Yang *et al* 2025). Recently, however, it has been suggested that dust emissions from interior sources on the TP are comparable to those of northern China, with both areas suggested to produce approximately 130 Tg of dust annually (Du *et al* 2022). In our data, the TP accounts for approximately 15% of all recorded dust events across East Asia, with average activation rates <1% of days with the remaining 85% of dust events occurring in northern China (i.e. our northern and southern source regions), with average activation rates of 1% and 3% of days, respectively (figure 2(a)).

Our data show that winter into earliest spring (i.e. December–March) is the primary dust season on the TP (figures 3(g) and (h)). We identify three principle TP dust sources (figures 8(a) and (b)): (i) the northern TP (80–94° E, 35–37° N, covering the northern part of the Changtang Plateau, the Hoh Xil Plateau, and the Qd B), with dust activation average at ∼5% of winter days; (ii) the central TP (80–93° E, 31–35° N, including the Ali Valley between Changtang Plateau and Gangdise Mts), with activation average at ∼3% of winter days; and (iii) the southern TP (82–93° E, 28–30° N, especially the Yarlung Zangbo River Valley), with an activation on ∼8% of winter days.

One exceptionally dust-active hotspot in the northern TP source is Zonag Lake (figure 2(f)) on the Hoh Xil Plateau (activation on ∼27% of winter days) (figure 8(b)). Here, extreme precipitation in 2011 triggered a flood that led to extensive erosion

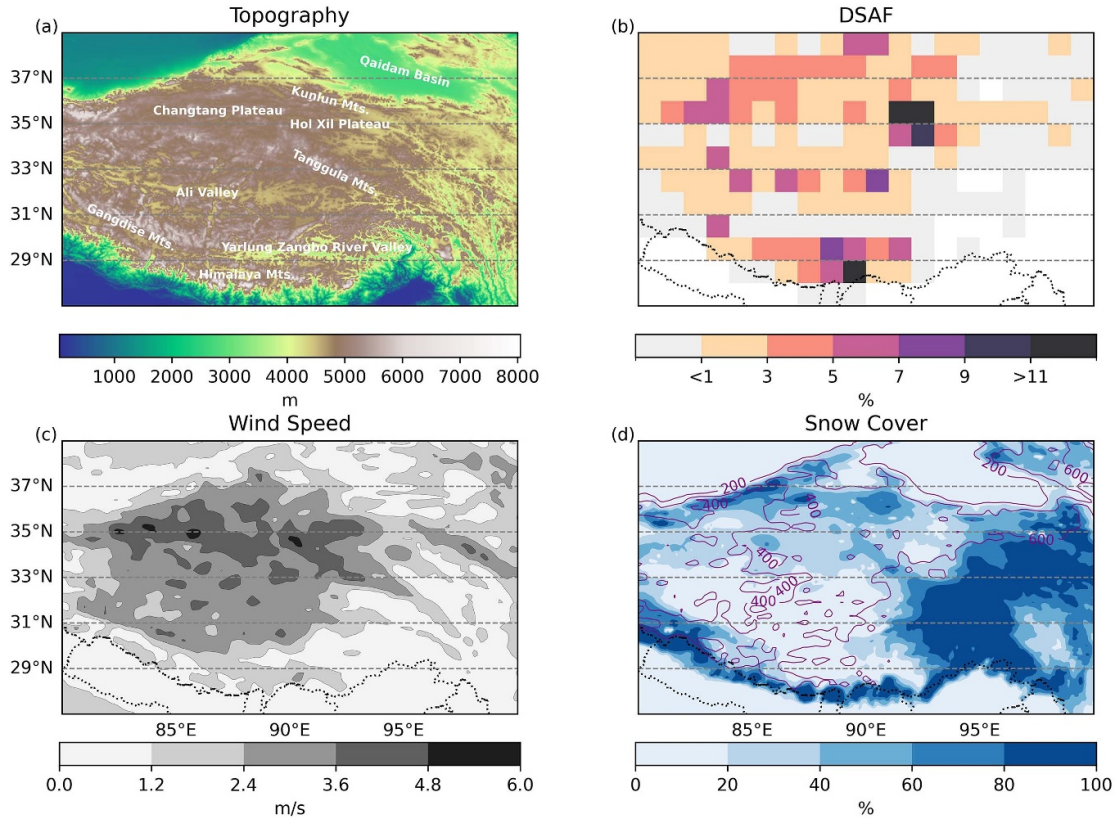

Figure 8. Controls on winter dust source activation frequency (DSAF) on the Tibetan Plateau. (a) Topography with mountain ranges and valleys labelled in white. (b) winter DSAF, (c) winter wind speed distribution and (d) winter snow cover distribution with annual precipitation in purple contour, all averaged over the study period (2016–2023). Snow cover, wind speed and precipitation are reconstructed from European Centre for Medium-Range Weather Forecasts Reanalysis 5 (ERA5) data (average for 2016–2023).

and deposition of a large sediment-rich area that is now exposed and an active dust-source (Lu *et al* 2020b). The flood also caused thermal alteration of the freeze–thaw cycle, the melting of ground ice and the destabilization of soil in the downstream region (Lu *et al* 2020a). These processes accelerated permafrost degradation and increased the potential for dust emissions.

The topography of the TP influences DSAF, with high DSAFs observed in low-elevation depositional environments such as the Ali valley (activation on ∼3% of winter days) and Yarlung Zangbo River Valley (activation on ∼8% of winter days) (figures 8(a) and (b)) because these basins generally act as depositional environments (Zender *et al* 2003). From northwest to southeast, winds weaken while precipitation and snow cover both increase (figures 8(c) and (d)), leading to a decrease of DSAF from the Changtang Plateau (figure 8(b)) toward the southeast, closely resembling the modeled dust flux distribution (Du *et al* 2022). Extreme topographic variation in the Yarlung Zangbo River Valley, one of the world's deepest river gorges with depths reaching up to 5,000 meters, also contributes to the very high DSAF values recorded here. During winter, river levels fall, exposing sandbanks and floodplains (Yang *et al* 2025) and the narrow and deep morphology of the valley helps channel winds, lifting loose soil and fine particles from the exposed areas of the valley floor (Zhang *et al* 2018).

Permafrost has been suggested to reduce the susceptibility of the land surface to deflation through ice cementation of mineral particles in soil pores, thereby increasing the threshold wind velocity required for sediment entrainment (Bullard *et al* 2016). Permafrost is extensively developed across the TP, particularly on the Changtang Plateau (supplementary figure 3). However, our winter DSAF data indicate that Changtang Plateau is a DSAF hotspot with activation on ∼4% of winter days (figures 8(a) and (b)). We infer that the extremely dry and windy conditions on the Changtang Plateau (annual precipitation 200–400 mm) lead to extremely low soil moisture levels and permafrost characterized by limited pore-ice, making deflation of mineral dust still possible in winter (figures 8(c) and (d)).

4. Conclusions

Dust storms in East Asia affect the health and livelihoods of hundreds of millions of people. We present the results of a systematic study of their sources and activation frequency for a region spanning 80–130° E and 27–52° N from January 2016 to December 2023

based on skilled human analysis of over 420 thousand satellite images. We draw the following conclusions:

(1) East Asia shows striking seasonal changes in both overall dust source activation frequency and in the latitudinal distribution of these events.
(2) There are two primary dust source regions in East Asia: a southern source region centered on the margins of the TK and a northern source region centered on the valleys of the Gobi Desert. The presence of lakes and paleolake remnants in both regions, especially in the TK (e.g. the Lop Nur, and the Tarim River, the Hetain River) promote DSAF hotspots.
(3) The AP (in the southern source region) is dust-active throughout the year. In this area and its adjacent regions, dry lakes, such as Gashun Nor, exhibit the highest DSAF, followed by oasis areas and croplands along the Hexi Corridor. The sandy deserts in this region are much less dust-active and the Chinese LP is almost completely inactive as a dust source.
(4) The Tibetan Plateau is not only a sink for wind-blown dust supplied from elsewhere; it is also an active dust source in winter and earliest spring. Here, precipitation patterns, snow cover and funneling of winds through steep river gorges all control activation.
(5) The Mongolian Plateau (in the northern source region) is a significant dust source in spring. Snow cover limits the northernmost extent of dust emissions in February. Vegetation suppresses dust emissions across the Mongolian Plateau, particularly in its northeastern region from April through May. The bare lands, grasslands and croplands of the region are all susceptible to dust source activation. The record-breaking Siberian heatwave of 2020 was associated with a spike in DSAF on the Mongolian Plateau over grasslands where livestock overgrazing is well documented.

The seasonal and latitudinal signals in our data, together with the anomaly associated with the 2020 heatwave, illustrate the power of our data set for quantifying modern dust source activation on observed human timescales. Our data also offer a framework to help evaluate past variabilities that have undoubtedly occurred on historical and geological timescales and to assess future change.

Data availability statement

The Himawari-8/9 data were obtained from the P-Tree System, operated by the Japan Aerospace Exploration Agency (JAXA) (www.eorc.jaxa.jp/ptree/). The ECMWF ERA5 climate reanalysis data were accessed through the Copernicus Climate Change Service Climate Data Store (https://cds.climate.copernicus.eu/datasets/). MODIS MCD12C1 Version 6.1 land cover data were obtained from the Land Processes Distributed Active Archive Center (https://lpdaac.usgs.gov/products/mcd12c1v061/). The livestock data is obtained from the National Statistical Office of Mongolia (www.1212.mn/en).

All data that support the findings of this study are included within the article (and any supplementary files).

Acknowledgments

The Himawari L1 Gridded data (produced from Himawari-8/9) used in this paper was supplied by the P-Tree System, Japan Aerospace Exploration Agency (JAXA). We acknowledge the use of the IRIDIS High Performance Computing Facility, and associated support services at the University of Southampton, in the completion of this work. We also thank Duo Chan for his assistance with IRIDIS. This work was supported by the Natural Environment Research Council (studentship NE/S007210/1 to LC through the INSPIRE Doctoral Training Programme).

ORCID iDs

Lingle Chen https://orcid.org/0000-0002-3525-9480
Kerstin Schepanski https://orcid.org/0000-0002-1027-6786
Anya J Crocker https://orcid.org/0000-0001-9561-5750
Chuang Xuan https://orcid.org/0000-0003-4043-3073
Paul A Wilson https://orcid.org/0000-0001-6425-8906

References

Akihiro S 2020 Introduction to Himawari-8 RGB composite imagery *Meteorological Satellite Center Technical Note 65*. (https://doi.org/10.1177/0379572120967819)
AlNasser F and Entekhabi D 2024 DustSCAN: a five year (2018–2022) hourly dataset of dust plumes from SEVIRI *Sci. Data* **11** 607
Altausen D *et al* 2019 Large-scale dust event in East Asia, as revealed by the Himawari-8 DUST RGB, lidar network observations, and field survey *E3S Web Conf.* **99** 01004
An L *et al* 2018 Temporal and spatial variations in sand and dust storm events in East Asia from 2007 to 2016: relationships with surface conditions and climate change *Sci. Total Environ.* **633** 452–62
Banks J R, Hünerbein A, Heinold B, Brindley H E, Deneke H and Schepanski K 2019 The sensitivity of the colour of dust in MSG-SEVIRI Desert Dust infrared composite imagery to surface and atmospheric conditions *Atmos. Chem. Phys.* **19** 6893–911
Bessho K *et al* 2016 An introduction to Himawari-8/9—Japan's new-generation geostationary meteorological satellites *J. Meteorol. Soc. Japan II* **94** 151–83
Bullard J E *et al* 2016 High-latitude dust in the Earth system *Rev. Geophys.* **54** 447–85

Chen Y, Takeuchi K, Xu C, Chen Y and Xu Z 2006 Regional climate change and its effects on river runoff in the Tarim Basin, China *Hydrol. Process.* **20** 2207–16
Ciavarella A *et al* 2021 Prolonged Siberian heat of 2020 almost impossible without human influence *Clim. Change* **166** 9
Dong Z, Lv P, Qian G, Xia X, Zhao Y and Mu G 2012 Research progress in China's Lop Nur *Earth Sci. Rev.* **111** 142–53
Du H, Xue X, Wang T, Lu S, Liao J, Li S, Fan Y and Liu X 2022 Modeling dust emission in alpine regions with low air temperature and low air pressure—A case study on the Qinghai-Tibetan Plateau (QTP) *Geoderma* **422** 115930
Ginoux P, Prospero J M, Gill T E, Hsu N C and Zhao M 2012 Global-scale attribution of anthropogenic and natural dust sources and their emission rates based on MODIS Deep Blue aerosol products *Rev. Geophys.* **50** RG3005
Ginoux P, Prospero J M, Torres O and Chin M 2004 Long-term simulation of global dust distribution with the GOCART model: correlation with North Atlantic Oscillation *Environ. Modell. Softw.* **19** 113–28
Han Y, Fang X, Kang S, Wang H and Kang F 2008 Shifts of dust source regions over central Asia and the Tibetan Plateau: connections with the Arctic oscillation and the westerly jet *Atmos. Environ.* **42** 2358–68
Hao Y, Wang Z, Xue L, Lou S, Ding K, Qin Y and Huang X 2024 Modeling the Effects of Vegetation and Snow on Dust Storm Over the Gobi Desert *J. Geophys. Res.* **129** e2024JD041407
Hennen M, White K and Shahgedanova M 2019 An assessment of SEVIRI imagery at various temporal resolutions and the effect on accurate dust emission mapping *Remote Sens.* **11** 918
Huang J, Wang T, Wang W, Li Z and Yan H 2014 Climate effects of dust aerosols over East Asian arid and semiarid regions *J. Geophys. Res.* **119** 11–398
Huang Z, Huang J, Hayasaka T, Wang S, Zhou T and Jin H 2015 Short-cut transport path for Asian dust directly to the Arctic: a case study *Environ. Res. Lett.* **10** 114018
Kai K, Kawai K, Ito A, Aizawa Y, Minamoto Y, Munkhjargal E and Davaanyam E 2021 Dust Hotspot in the Gobi Desert: a Field Survey in April 2019 *Sola* **17** 130–3
Kim C-H and Lee H-J 2013 Numerical simulations of Asian dust events: a Lagrangian Dust Model and its applications *Asia-Pac. J. Atmos. Sci.* **49** 571–86
Kok J F *et al* 2021 Contribution of the world's main dust source regions to the global cycle of desert dust *Atmos. Chem. Phys.* **21** 8169–93
Kok J F, Storelvmo T, Karydis V A, Adebiyi A A, Mahowald N M, Evan A T, He C and Leung D M 2023 Mineral dust aerosol impacts on global climate and climate change *Nat. Rev. Earth Environ.* **4** 71–86
Kunkelova T *et al* 2022 Dust sources in Westernmost Asia have a different geochemical fingerprint to those in the Sahara *Q. Sci. Rev.* **294** 107717
Kunkelova T, Crocker A J, Wilson P A and Schepanski K 2024 Dust source activation frequency in the Horn of Africa *J. Geophys. Res.* **129** e2023JD039694
Kurosaki Y and Mikami M 2003 Recent frequent dust events and their relation to surface wind in East Asia *Geophys. Res. Lett.* **30** 1736
Kurosaki Y and Mikami M 2004 Effect of snow cover on threshold wind velocity of dust outbreak *Geophys. Res. Lett.* **31** L03106
Lee J-J and Kim C-H 2012 Roles of surface wind, NDVI and snow cover in the recent changes in Asian dust storm occurrence frequency *Atmos. Environ.* **59** 366–75
Lehmkuhl F, Grunert J, Hülle D, Batkhishig O and Stauch G 2018 Paleolakes in the Gobi region of southern Mongolia *Q. Sci. Rev.* **179** 1–23
Lehmkuhl F, Wolf D, Boemke B, Klinge M, Batkhishig O and Grunert J 2024 Aeolian sediments in western Mongolia: distribution and (paleo)climatic implications *Geomorphology* **465** 109407
Li F-R, Zhao L-Y, Zhang H, Zhang T-H and Shirato Y 2004 Wind erosion and airborne dust deposition in farmland during spring in the Horqin Sandy Land of eastern Inner Mongolia, China *Soil Tillage Res.* **75** 121–30
Lim J-Y and Chun Y 2006 The characteristics of Asian dust events in Northeast Asia during the springtime from 1993 to 2004 *Glob. Planet. Change* **52** 231–47
Lu P, Han J, Li Z, Xu R, Li R, Hao T and Qiao G 2020a Lake outburst accelerated permafrost degradation on Qinghai-Tibet Plateau *Remote Sens. Environ.* **249** 112011
Lu S, Chen F, Zhou J, Hughes A C, Ma X and Gao W 2020b Cascading implications of a single climate change event for fragile ecosystems on the Qinghai-Tibetan Plateau *Ecosphere* **11** e03243
Luo H, Guan Q, Pan N, Wang Q, Li H, Lin J, Tan Z and Shao W 2020 Using composite fingerprints to quantify the potential dust source contributions in northwest China *Sci. Total Environ.* **742** 140560
Nandintsetseg B, Boldgiv B, Chang J, Ciais P, Davaanyam E, Batbold A, Bat-Oyun T and Stenseth N C 2021 Risk and vulnerability of Mongolian grasslands under climate change *Environ. Res. Lett.* **16** 034035
Nandintsetseg B and Shinoda M 2015 Land surface memory effects on dust emission in a Mongolian temperate grassland *J. Geophys. Res.* **120** 414–27
Natsagdorj L, Jugder D and Chung Y S 2003 Analysis of dust storms observed in Mongolia during 1937–1999 *Atmos. Environ.* **37** 1401–11
Nobakht M, Shahgedanova M and White K 2021 New inventory of dust emission sources in Central Asia and Northwestern China derived from MODIS imagery using dust enhancement technique *J. Geophys. Res.* **126** e2020JD033382
Prospero J M, Ginoux P, Torres O, Nicholson S E and Gill T E 2002 Environmental characterization of global sources of atmospheric soil dust identified with the Nimbus 7 Total Ozone Mapping Spectrometer (Toms) ABSORBING AEROSOL PRODUCt *Rev. Geophys.* **40** 2–1
Pye K and Zhou L-P 1989 Late Pleistocene and Holocene aeolian dust deposition in north China and the northwest Pacific Ocean *Palaeogeograph. Palaeoclimatol. Palaeoecol.* **73** 11–23
Qian W, Quan L and Shi S 2002 Variations of the dust storm in China and its climatic control *J. Clim.* **15** 1216–29
Rittner M *et al* 2016 The provenance of Taklamakan desert sand *Earth Planet. Sci. Lett.* **437** 127–37
Schär C, Lüthi D and Schiemann R 2009 Seasonality and Interannual Variability of the Westerly Jet in the Tibetan Plateau Region* *J. Clim.* **22** 2940–57
Schepanski K, Tegen I, Laurent B, Heinold B and Macke A 2007 A new Saharan dust source activation frequency map derived from MSG-SEVIRI IR-channels *Geophys. Res. Lett.* **34** L18803
Schepanski K, Tegen I and Macke A 2012 Comparison of satellite based observations of Saharan dust source areas *Remote Sens. Environ.* **123** 90–97
Shao Y and Dong C H 2006 A review on East Asian dust storm climate, modelling and monitoring *Glob. Planet. Change* **52** 1–22
Shen Y, Shen Z, Du M and Wang W 2005 Dust emission over different land surface in the arid region of northwest China *J. Meteorol. Soc. Japan II* **83** 935–42
Shinoda M, Kimura R, Mikami M, Tsubo M, Nishihara E, Ishizuka M, Yamada Y, Munkhtsetseg E, Jugder D and Kurosaki Y 2010 Characteristics of dust emission in the mongolian steppe during the 2008 DUVEX intensive observational period *Sola* **6** 9–12
Sun J, Zhang M and Liu T 2001 Spatial and temporal characteristics of dust storms in China and its surrounding regions, 1960–1999: relations to source area and climate *J. Geophys. Res.* **106** 10325–33
Tanaka T Y, Sekiyama T T, Maki T and Mikami M 2011 The effects of snow cover and soil moisture on Asian Dust: i. A numerical sensitivity study *Sola* **7A** 36–39

Wang R-D, Li Q, Zhang C-L, Wang Z-T, Guo Z-L, Chang C-P and Li J-F 2021 Comparison of dust emission ability of sand desert, gravel desert (Gobi), and farmland in northern China *Catena* **201** 105215

Wang S, Wang J, Zhou Z and Shang K 2005 Regional characteristics of three kinds of dust storm events in China *Atmos. Environ.* **39** 509–20

Wang T, Yan C Z, Song X and Li S 2011 Landsat images reveal trends in the Aeolian Desertification in a Source Area for Sand and Dust Storms in China's Alashan Plateau (1975–2007) *Land Degrad. Dev.* **24** 422–9

Wang Y, Jia J, Lu H, Lu C and Xia D 2019 Fluvial sediments in the Alagxa Plateau as a dust source: iron mineralogical and geochemical evidence *J. Arid Land* **11** 217–27

Wu J, Kurosaki Y, Shinoda M and Kai K 2016 Regional characteristics of recent dust occurrence and its controlling factors in East Asia *Sola* **12** 187–91

Xuan J and Sokolik I N 2002 Characterization of sources and emission rates of mineral dust in Northern China *Atmos. Environ.* **36** 4863–76

Xuan J, Sokolik I N, Hao J, Guo F, Mao H and Yang G 2004 Identification and characterization of sources of atmospheric mineral dust in East Asia *Atmos. Environ.* **38** 6239–52

Yang J *et al* 2025 Spatiotemporal evolution of aeolian sedimentary landscapes on the southern Tibetan Plateau during the late Quaternary: a review and recent advances *Earth Sci. Rev.* **261** 105035

Yu Y, Kalashnikova O V, Garay M J and Notaro M 2019 Climatology of Asian dust activation and transport potential based on MISR satellite observations and trajectory analysis *Atmos. Chem. Phys.* **19** 363–78

Yumimoto K, Kajino M, Tanaka T Y and Uno I 2019 Dust vortex in the Taklimakan Desert by Himawari-8 High Frequency and Resolution Observation *Sci. Rep.* **9** 1209

Zdanowicz C, Hall G, Vaive J, Amelin Y, Percival J, Girard I, Biscaye P and Bory A 2006 Asian dustfall in the St. Elias Mountains, Yukon, Canada *Geochim. Cosmochim. Acta* **70** 3493–507

Zender C S, Bian H and Newman D 2003 Mineral Dust Entrainment and Deposition (DEAD) model: description and 1990s dust climatology *J. Geophys. Res.* **108** 4416

Zhang B, Tsunekawa A and Tsubo M 2008 Contributions of sandy lands and stony deserts to long-distance dust emission in China and Mongolia during 2000–2006 *Glob. Planet. Change* **60** 487–504

Zhang B, Tsunekawa A and Tsubo M 2015a Identification of dust hot spots from Multi-Resolution Remotely Sensed Data in Eastern China and Mongolia *Water Air Soil Pollut.* **226** 117

Zhang C L, Li Q, Shen Y P, Zhou N, Wang X S, Li J and Jia W R 2018 Monitoring of aeolian desertification on the Qinghai-Tibet Plateau from the 1970s to 2015 using Landsat images *Sci. Total Environ.* **619–620** 1648–59

Zhang X, Zhou Q, Chen W, Wang Y and Tong D Q 2015b Observation and modeling of black soil wind-blown erosion from cropland in Northeastern China *Aeolian Res.* **19** 153–62

Zhang Z *et al* 2023 Quantifying mineral dust emissions on the Tibetan Plateau with a modified dust source map *Geophys. Res. Lett.* **51** e2023GL107042

Zhang Z, Bird A, Zhang C and Dong Z 2022 Not all gravel deserts in northern China are sources of regionally deposited dust *Atmos. Environ.* **273** 118984